A TIME ACCURATE ZONAL FINITE ELEMENT METHOD FOR SOLVING COMPRESSIBLE AND INCOMPRESSIBLE VISCOUS FLOWS

Jichao Su
Aerodynamics Laboratory, Institute for Aerospace Research,
National Research Council Canada, Ottawa, Ontario, K1A 0R6, Canada

Keywords: *finite element method, zonal method, viscous flow, aerodynamics*

Abstract

A time accurate viscous-inviscid zonal method is presented for simulating compressible and incompressible external aerodynamic viscous flows. The division of the flow field into inviscid and viscous zones is warranted by the physical nature of the problems. However making full use of such division is the motivation of the present method.

A finite element method is used to solve both the inviscid and viscous problems. The inviscid solution is computed by solving the potential flow with a density upwind (also called artificial compressibility) finite element method. The viscous solution is obtained by solving the Reynolds-averaged Navier-Stokes (RANS) equations via a streamline upwind Petrov-Galerkin finite element method.

Numerical results are presented for two-dimensional compressible and incompressible high Reynolds number turbulent flows around NACA 0012 and RAE 2822 airfoils. The results obtained with the present viscous-inviscid method are in good agreement with the full Navier-Stokes solutions of the present author and other researchers.

1 Introduction

Difficulties encountered in the simulation of fluid flows, especially aerodynamic flows, are usually related to the existence of very different length and time scales in different flow regions such as the inviscid flow region, viscous thin layer and shock wave. When handling this type of challenge, commonly referred to the stiffness of the governing equations, by most numerical algorithms and methods, special care must be taken for grid generation, turbulence modeling as well as solving the equations and many other issues. The aerodynamic flow around an aircraft is a typical example of the above difficulties. This stiffness of the governing equations may also be an indication that dealing with different flow regions by different approaches might be wiser, more efficient and revealing. For an aerodynamic problem, although the flow is governed by the Navier-Stokes equations, the vast portion of the flow field around the aircraft, where the viscous effects are not important, can be well represented by a potential or Euler solution. Viscosity is important only in a very thin layer close to the aircraft surface for attached flows. Even for large separated flows, the substantial viscous effects are restricted to the region near the aircraft surface and in its wake. Therefore, from an application perspective, a natural solution procedure would be based on a viscous-inviscid splitting approach [1-7]. This approach consists of dealing with different regions of the flow in different ways by taking advantage of the flow nature in each region. The early viscous-inviscid interactive boundary layer method is the best example of this philosophy. The approximations to the Navier-Stokes equations of the early boundary layer method limited its application range. However, a viscous-inviscid splitting approach does not necessarily mean the degradation in the accuracy of the solution compared to a RANS solution method [3-10].

Researchers such as Brune, et al [8], Cambier, et al [9], and Le Balleur [3-7] should be mentioned amongst others for their contributions to the viscous-inviscid splitting approach. Specially, major contributions have been made by Le Balleur to bring the approach to the stage of engineering applications. Le Balleur started his research on a viscous-inviscid splitting method in late 1970s. Through decades of research, he has developed a sophisticated and yet efficient method with a strong physical insight to deal with high Reynolds number external turbulent flows. In his viscous-inviscid splitting method, Le Balleur introduced a defect-formulation theory that is the key for his subsequent derivations of integral forms of the governing equations and handling of the coupling between viscous and inviscid solutions [3-7]. With a thin-layer approximation and introduction of a parametric velocity profile model, he was able to solve, at much lower cost, large separated flows around three-dimensional configurations [6]. He has applied his method to two and three dimensional, compressible and incompressible, steady and unsteady, high Reynolds number external flows.

The viscous-inviscid zonal method presented in this paper is one type of the viscous-inviscid splitting approach. In the zonal method, the computational domain is divided into an inviscid zone where an inviscid solver is used and a viscous zone near the body surface and its wake where a RANS solver is employed to deal with the turbulent flow. The computational efficiency is thus improved by reducing the extent of the viscous computational domain [8-10]. The RANS solver must be coupled with the inviscid solver along a patching boundary, located in the inviscid part of the flow.

As far as the space discretization is concerned, in the present paper, the finite element method [11-14] is used to address both the inviscid and viscous problems. The inviscid solution is computed by solving the potential flow equation with a density upwind finite element method. The viscous solution is obtained by solving the RANS equations via an inconsistent streamline upwind Petrov-Galerkin finite element method that can be regarded, as shown in the present paper, as a Galerkin method applied to a modified governing equation. The Spalart-Allmaras one-equation turbulence model is employed in this study because of its success in solving the aerodynamic flow problems.

The present zonal method has been previously applied, by the author [10], to two-dimensional compressible and incompressible low Reynolds number flows. In the current study, the author has further extended and applied the method to two-dimensional compressible and incompressible high Reynolds number turbulent flows.

2 Governing Equations and Numerical Method

2.1 Navier-Stokes viscous solution method

In the present study, we consider two-dimensional compressible and incompressible viscous flows around an airfoil. For these flows, the governing equations take the following form:

$$\frac{\partial \rho}{\partial t}+\frac{\partial(\rho u_i)}{\partial x_i}=0 \tag{1}$$

$$\frac{\partial(\rho u_j)}{\partial t}+\frac{\partial(\rho u_i u_j)}{\partial x_i}=-\frac{\partial p}{\partial x_j}+\frac{\partial t_{ij}}{\partial x_j} \quad (j=1,2) \tag{2}$$

$$\frac{\partial}{\partial t}\left[\rho\left(h+\frac{1}{2}u_i u_i\right)\right]+\frac{\partial}{\partial x_j}\left[\rho u_j\left(h+\frac{1}{2}u_i u_i\right)\right] =\frac{\partial p}{\partial t}+\frac{\partial(u_i t_{ij})}{\partial x_j}-\frac{\partial q_j}{\partial x_j} \tag{3}$$

where $e=C_v T$ is the specific internal energy and C_v is the specific heat coefficient; $h=e+p/\rho$ is the specific enthalpy; the repeated indices indicate summation. The heat flux vector q_j is governed by Fourier's law

$$q_j=-\kappa\frac{\partial T}{\partial x_j} \quad (j=1,2) \tag{4}$$

where κ is the thermal conductivity. The perfect gas law

$$p = \rho RT \tag{5}$$

and the constitute relation between stress and strain rate

$$\begin{aligned} t_{ij} &= 2\mu S_{ij} - \frac{2}{3}\mu \frac{\partial u_k}{\partial x_k}\delta_{ij} \\ S_{ij} &= \frac{1}{2}\left(\frac{\partial u_i}{\partial x_j} + \frac{\partial u_j}{\partial x_i}\right) \end{aligned} \tag{6}$$

close the above system. Here, R is the perfect gas constant and δ_{ij} is the Kronecker delta. The thermal conductivity is determined by $\kappa = \frac{\gamma}{\gamma-1} R\mu / Pr$, where Pr is the Prandtl number and γ is the ratio of specific heats.

An implicit operator-splitting algorithm is employed to solve the above momentum equations. The algorithm essentially splits the velocity components into two parts such that the continuity equation and pressure terms in the momentum equations can be treated separately. In the algorithm, ρu_j is divided in the time interval from t_n to t_n+dt as

$$\begin{aligned} &\rho u_j(x_1,x_2,t) = (\rho u_j)_n(x_1,x_2) \\ &+\Delta(\rho u_j)^*(x_1,x_2,t) + \Delta(\rho u_j)^{**}(x_1,x_2,t) \end{aligned} \quad (j=1,2) \tag{7}$$

and the pressure p is expressed as

$$p(x_1,x_2,t) = p_n(x_1,x_2) + \Delta p(x_1,x_2,t) \tag{8}$$

where $\Delta(\rho u_j)^*, \Delta(\rho u_j)^{**} (j=1,2)$ and Δp are incremental values as yet to be determined. Substituting equations (7) and (8) in the momentum equation (2), we can split the momentum equation into two equations as

$$\frac{\partial(\Delta(\rho u_j)^*)}{\partial t} + \frac{\partial(\rho u_i u_j)}{\partial x_i} = -\frac{\partial p_n}{\partial x_j} + \frac{\partial t_{ij}}{\partial x_j} \quad (j=1,2) \tag{9}$$

$$\frac{\partial(\Delta(\rho u_j)^{**})}{\partial t} + \frac{\partial(\Delta p)}{\partial x_j} = 0 \tag{10}$$

From equation (10), we note that $\Delta(\rho u_j)^{**}$ is associated with the increment of pressure p. This equation may be regarded as a correction equation that ensures the satisfaction of mass continuity.

A fully implicit algorithm is developed for the solution of equation (9) that is further replaced by a non-conservative form by making use of the continuity equation. Discretizing the resulting non-conservative equation in time, we obtain

$$\begin{aligned} &\rho_n(\Delta u_j)^*_{n+1} - \theta\Delta t \frac{\partial(\Delta t_{ij})^*_{n+1}}{\partial x_j} + \theta\Delta t(\rho u_i)_n \frac{\partial(\Delta u_j)^*_{n+1}}{\partial x_i} \\ &= -\Delta t\left[(\rho u_i)_n \frac{\partial(u_j)_n}{\partial x_i} + \frac{\partial p_n}{\partial x_j} - \frac{\partial(t_{ij})_n}{\partial x_j}\right] (j=1,2) \end{aligned} \tag{11}$$

where

$$\begin{aligned} (\Delta t_{ij})^*_{n+1} &= 2\mu(\Delta S_{ij})^*_{n+1} - \frac{2}{3}\mu\frac{\partial(\Delta u_k)^*_{n+1}}{\partial x_k}\delta_{ij} \\ (\Delta S_{ij})^*_{n+1} &= \frac{1}{2}\left(\frac{\partial(\Delta u_i)^*_{n+1}}{\partial x_j} + \frac{\partial(\Delta u_j)^*_{n+1}}{\partial x_i}\right) \end{aligned} \tag{12}$$

Equation (11) is then solved by an inconsistent streamline upwind Petrov-Galerkin finite element method [14].

A prescribed Dirichlet velocity boundary condition is implemented for the first part of the solution. That is

$$(\Delta u_j)^* = \bar{u}_j(x_1,x_2,t) - \bar{u}_j(x_1,x_2,t_n) \quad (j=1,2) \text{ on } \partial\Omega \tag{13}$$

where $\partial\Omega$ is the boundary of the fluid domain of investigation, Ω, and $\bar{u}_j$ denotes the prescribed value on the boundary. For the second part of the solution we impose homogeneous boundary conditions, namely,

$$\Delta(\rho u_j)^{**} = 0 \quad (j=1,2) \text{ on } \partial\Omega \tag{14}$$

so that the combination of the two parts of the solution satisfies the given physical boundary conditions.

Equations (10) and (1) are required for the solution of $\Delta(\rho u_j)^{**}$ and Δp. With discretizing both equations in time and a little derivation, we obtain

$$\begin{aligned} &\frac{1}{RT_n}(\Delta p)_{n+1} - (\theta\Delta t)^2\nabla^2(\Delta p)_{n+1} \\ &= -\Delta t\left[\frac{\partial(\rho u_i)_n}{\partial x_i} + \theta\frac{\partial(\Delta(\rho u_i)^*_{n+1})}{\partial x_i}\right] \end{aligned} \tag{15}$$

$$\Delta(\rho u_j)^{**}_{n+1} = -\theta\Delta t\frac{\partial(\Delta p)_{n+1}}{\partial x_j} \quad (j=1,2) \tag{16}$$

where ∇ is the gradient operator. These two equations with the following boundary conditions

$$\Delta(\rho u_j)^{**}_{n+1} = 0 \quad (j = 1,2) \text{ on } \partial\Omega \tag{17}$$

$$\frac{\partial(\Delta p)_{n+1}}{\partial \bar{n}} = 0 \quad \text{on } \partial\Omega \tag{18}$$

determine the solution of $\Delta(\rho u_j)^{**}$ and Δp. $\bar{n}$ denotes the normal to the boundary. The discretization of equation (3) is similar to that of equation (9).

When turbulent flows are considered and a turbulence model is introduced, the viscosity μ in equations (2) and (3) is replaced by $\mu + \mu_T$ where μ_T is the eddy viscosity as defined below, and κ is replaced by $\kappa + \kappa_T$ where $\kappa_T = \frac{\gamma}{\gamma - 1} R\mu_T / \mathrm{Pr}_T$ with Pr_T being the turbulent Prandtl number. In the present study, the Spalart-Allmaras one equation model is employed to compute the eddy viscosity [15]. Its defining equations are as follows:

$$\nu_T = \bar{\nu} f_{\upsilon 1}; \quad \mu_T = \rho \nu_T \tag{19}$$

$$\frac{\partial \bar{\nu}}{\partial t} + \frac{\partial (u_i \bar{\nu})}{\partial x_i} = c_{b1} \bar{S} \bar{\nu} - c_{w1} f_w \left(\frac{\bar{\nu}}{d} \right)^2 + \frac{1}{\sigma} \frac{\partial}{\partial x_i} \left[(\nu + \bar{\nu}) \frac{\partial \bar{\nu}}{\partial x_i} \right] + \frac{c_{b2}}{\sigma} \frac{\partial \bar{\nu}}{\partial x_i} \frac{\partial \bar{\nu}}{\partial x_i} \tag{20}$$

where d is the distance to the closest surface and the kinematic viscosity is $\nu = \mu / \rho$. The definition of the closure coefficients and auxiliary relations can be found in [10,15].

The time discretization of equation (20) is similar to that of equation (9), however, care should be taken with its spatial discretization. To ensure a positive matrix operator that guarantees a non-negative eddy viscosity, following the suggestion by Spalart and Allmaras [13], equation (20) is rearranged as

$$\frac{\partial \bar{\nu}}{\partial t} + \frac{\partial (u_i \bar{\nu})}{\partial x_i} = c_{b1} \bar{S} \bar{\nu} - c_{w1} f_w \left(\frac{\bar{\nu}}{d} \right)^2 + \frac{1 + C_{b2}}{\sigma} \frac{\partial}{\partial x_i} \left[(\nu + \bar{\nu}) \frac{\partial \bar{\nu}}{\partial x_i} \right] - \frac{c_{b2}}{\sigma} (\nu + \bar{\nu}) \frac{\partial^2 \bar{\nu}}{\partial x_i \partial x_i} \tag{21}$$

where the differentiation of the molecular viscosity has been neglected. Using equation (21) instead of (20) avoids the discretization of the term $(\nabla \nu)^2$, which does not easily generate a positive discrete matrix operator.

2.2 Potential inviscid solution method

The full potential equation is the continuity equation (1) with the velocity defined as

$$u_j = (u_j)_\infty + \frac{\partial \phi}{\partial x_j} \tag{22}$$

and the density, pressure and temperature determined by

$$\rho = \rho_\infty \left[1 + \frac{\gamma - 1}{2} M_\infty^2 \left(1 - \frac{V^2 + 2\phi_t}{V_\infty^2} \right) \right]^{1/(\gamma - 1)} \tag{23}$$

$$p = p_\infty \left[1 + \frac{\gamma - 1}{2} M_\infty^2 \left(1 - \frac{V^2 + 2\phi_t}{V_\infty^2} \right) \right]^{\gamma/(\gamma - 1)} \tag{24}$$

$$T = T_\infty \left[1 + \frac{\gamma - 1}{2} M_\infty^2 \left(1 - \frac{V^2 + 2\phi_t}{V_\infty^2} \right) \right] \tag{25}$$

where $(u_j)_\infty$, ρ_∞, p_∞, T_∞, M_∞, and ϕ are the freestream velocity, density, pressure, temperature, Mach number, and the perturbation velocity potential, respectively; $V^2 = u_i u_i$; $\phi_t = \partial \phi / \partial t$. For incompressible flows, the density ρ is constant and thus the perturbation potential satisfies the Laplace equation. The boundary conditions for equations (1) and (22) are:

1. The perturbation velocity potential in the farfield (except at the outflow) is set to zero;

2. The flux through the outflow boundary is set equal to the freestream flux. This condition allows a jump in the velocity potential in the wake;

3. If the whole flow field is chosen as an inviscid potential zone, then additional conditions are required. At any location on a prescribed wake sheet, there are two values for ϕ, so two conditions must be imposed. First, the mass flux through the wake is continuous and second, the pressures on the upper and lower surfaces of the wake sheet must be equal.

A density upwind Galerkin finite element method [16,17] was used to solve the above potential flow problem. The basic concept of the density upwind is to replace the density in the continuity equation, when implementing the spatial discretization, by

$$\bar{\rho} = \rho - \sigma_f (\rho - \rho_{upwind}) \tag{26}$$

where ρ_{upwind} is the density at the upstream node of the current node and

$$\sigma_f = \sigma_c \max(0, \sigma)$$
$$\sigma = 1 - \frac{M^2_{critical}}{M^2} \quad (27)$$

where M is the local Mach number and $M_{critical}$ (≈ 0.98) is a critical Mach number defined to control the spatial extent of the upwind region. σ_c $(=1.0 \sim 3.0)$ is a parameter to control the amount of the upwind effect.

2.3 Match of the inner viscous and outer inviscid solutions

The interfaces that separate the inviscid and viscous zones are located in the inviscid domain and have two adjacent surfaces. The velocity, pressure and temperature are matched on these surfaces in such a way that the potential governing equation is satisfied on one surface while the viscous Navier-Stokes equations including the energy equation are satisfied on the other surface.

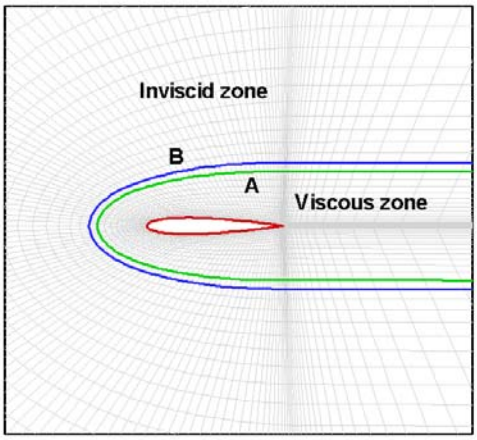

Fig. 1. A typical zonal C-grid around an airfoil

In figure 1, the interfaces are indicated by surfaces A and B. On surface A, a following potential boundary condition is implemented

$$\frac{\partial(\Delta\phi)}{\partial \bar{n}} = \bar{n}_i \Delta u_i \quad (28)$$

where $\bar{n}_i$ denotes the ith component of the unit outward normal to the boundary. On surface B, the Navier-Stokes boundary conditions below are imposed

$$\Delta u_i = \frac{\partial(\Delta\phi)}{\partial x_i} \quad (i = 1,2)$$
$$\Delta p = \Delta p_{potential} \quad (29)$$
$$\Delta T = \Delta T_{potential}$$

This also implies that the potential equation is satisfied on surface B while the NS equations are satisfied on surface A.

3 Numerical Implementation

A finite element method is employed to discretize the governing equations in space after the time discretization. For demonstration, equation (11) is considered. A weak formulation is obtained by taking a scalar product with an appropriate weighting function and integrating over the domain Ω. Then, for the discretization of the weak formulation we may use different or the same interpolation approximations for both velocity and pressure. In the present study, we use bilinear approximations for all variables. The interpolations are expressed as

$$u_j(x_1, x_2) = \sum_{i=1}^{\bar{N}} U_i(x_1, x_2)(u_j)_i \quad (j = 1,2) \quad (30)$$

$$p(x_1, x_2) = \sum_{i=1}^{\bar{M}} \Pi_i(x_1, x_2)\, p_i \quad (31)$$

where $\bar{N}$ is the total number of nodes for the velocity components; $\bar{M}$ is the total number of nodes for the pressure; $(u_j)_i$ and p_i are the nodal variables; $U_i(x_1, x_2)$ and $\Pi_i(x_1, x_2)$ are node functions. By using equations (30) and (31) and setting the weighting function the same as the corresponding node function (with an upwind modification for a Petrov-Galerkin method), we can derive a finite element algebraic system of equations, which is solved for the nodal variables.

A similar procedure is used for equations (15) and (16) for $\Delta(\rho u_j)^{**}$ and Δp, equation (21) for eddy viscosity, equations (1) and (24) for the velocity potential, and equation (3) for T.

Focusing on the streamline upwind Petrov-Galerkin method, the following derivation

shows its essence. A general form of a transport equation can be written as

$$\frac{\partial(\rho\varphi)}{\partial t}+\frac{\partial(\rho u_i\varphi)}{\partial x_i}=\frac{\partial}{\partial x_i}\left(k\frac{\partial\varphi}{\partial x_i}\right)+f \qquad (32)$$

To solve the above equation numerically, an upwind effect is generally required to make a solution stable in the spatial discretization when the convection terms dominate the solution. In a finite volume method, including upwind is quite straight forward and a variety of first-order or high-order schemes have been developed. However, in a finite element method, the common way of considering upwind effects is by modifying the weighting function; weighting upstream nodes more than downstream nodes [14]. Here we deal with the issue from a different perspective. We first modify equation (32) to include an upwind effect prior to spatial discretization. To achieve that, φ is replaced in the convection terms in the above equation by a Taylor expansion along the local streamline as

$$\bar{\varphi}=\varphi-\frac{h_s}{V}u_i\frac{\partial\varphi}{\partial x_i} \qquad (33)$$

where h_s controls the magnitude of the upwind effect and is defined below. Thus the modified non-conservative form of equation (32) is

$$\rho\frac{\partial\varphi}{\partial t}+\rho u_i\frac{\partial\varphi}{\partial x_i}-\frac{\partial}{\partial x_i}\left[\frac{h_s}{V}\rho u_i\left(u_j\frac{\partial\varphi}{\partial x_j}\right)\right] =\frac{\partial}{\partial x_i}\left(k\frac{\partial\varphi}{\partial x_i}\right)+f \qquad (34)$$

By applying a standard Galerkin method, we obtain a weak formulation as

$$\int_\Omega\Psi\left(\rho\frac{\partial\varphi}{\partial t}\right)d\Omega+\int_\Omega\left(\Psi+\frac{h_s}{V}u_j\frac{\partial\Psi}{\partial x_j}\right)\left(\rho u_i\frac{\partial\varphi}{\partial x_i}\right)d\Omega -\int_{\partial\Omega}\Psi\frac{h_s}{V}(u_j\bar{n}_j)\left(\rho u_i\frac{\partial\varphi}{\partial x_i}\right)d(\partial\Omega) \qquad (35)$$
$$=-\int_\Omega\frac{\partial\Psi}{\partial x_i}\left(k\frac{\partial\varphi}{\partial x_i}\right)d\Omega+\int_\Omega\Psi f d\Omega+\int_{\partial\Omega}\Psi\left(k\frac{\partial\varphi}{\partial\bar{n}}\right)d(\partial\Omega)$$

which is simply an inconsistent streamline upwind Petrov-Galerkin weak formulation if $u_i\bar{n}_i=0$ on the boundary of the fluid domain, where Ψ is a Galerkin weighting function. If the weighting function, applied to the convection term in the above equation, $\Psi+\frac{h_s}{V}u_j\frac{\partial\Psi}{\partial x_j}$, is applied to all the terms in equation (32) (in the non-conservative form), then a consistent streamline upwind Petrov-Galerkin weak formulation results. In this study, $h_s=\eta h_e$ at each node with h_e being the average of the maximum dimensions of the elements around the node and $\eta\approx 0.1$. This definition is different from that suggested by Brooks and Hughes [14].

4 Numerical Results and Discussion

Some calculated results are presented for two-dimensional compressible and incompressible flows around NACA 0012 and RAE 2822 airfoils. A typical C-type grid near the airfoil is shown in figure 1.

4.1 Incompressible flow

Figure 2 (where c is the airfoil chord length) shows the pressure coefficient on the surface of the NACA 0012 airfoil with 0^o angle of attack and a Mach numer of $M_\infty=0.0$. A 199x51 C-grid and its modifications in consideration of a

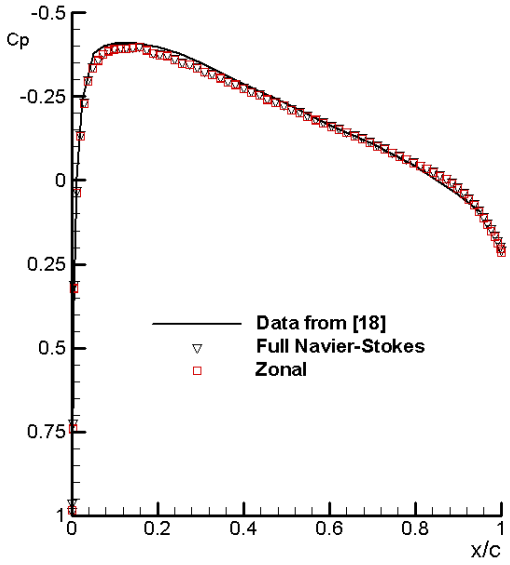

Fig. 2. Pressure coefficient over the NACA 0012 airfoil at $\alpha=0^o$, $M_\infty=0.0$ and Re=5x10^6.

certain angle of attack are, generated for the calculations of flows around the NACA 0012 airfoil. The 199x28 grid near the airfoil and its wake is chosen as the viscous zone and the 199x23 grid outside the viscous zone as the inviscid zone. When the whole grid is chosen as an inviscid zone, a potential solution is obtained. A full Navier-Stokes solution is calculated if the whole grid is chosen as a viscous zone. The first grid point off the wall is at a distance of about $1\text{x}10^{-5}$ chords, which provides a reasonable numerical resolution for the flows considered (guaranteeing a value of $y^+ = u_\tau y/\nu < 10$, where u_τ is the friction velocity). Both full Navier-Stokes and zonal solutions are shown in the figure for a viscous flow with a Reynolds number (Re) of $5\text{x}10^6$. The agreement is very good. The results are also in good agreement with the empirical data from [18].

4.2 Compressible flows

The numerical results for compressible flows around the NACA 0012 airfoil are shown in figures 3-5. The results for 10^o angle of attack, $M_\infty = 0.5$ and Re=$5\text{x}10^6$ are presented in figure 3. Again the full Navier-Stokes and zonal solutions are in excellent agreement for these viscous flows. For the case of zero angle of attack, M_∞=0.80 and Re=$9\text{x}10^6$, the result by the zonal method matches very well the full

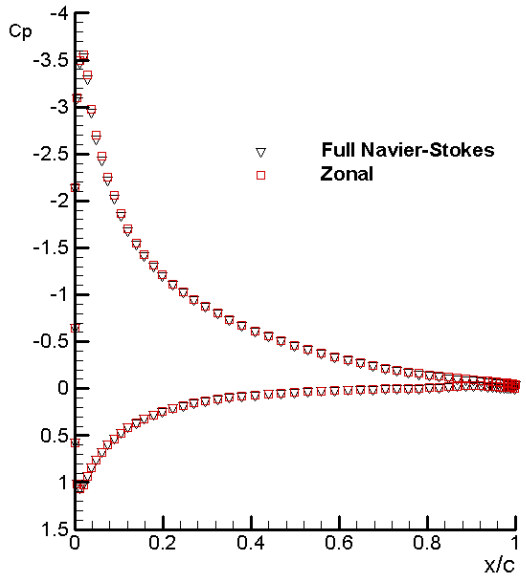

Fig. 3. Pressure coefficient over the NACA 0012 airfoil at $\alpha = 10^o$, $M_\infty = 0.5$ and Re=$5\text{x}10^6$.

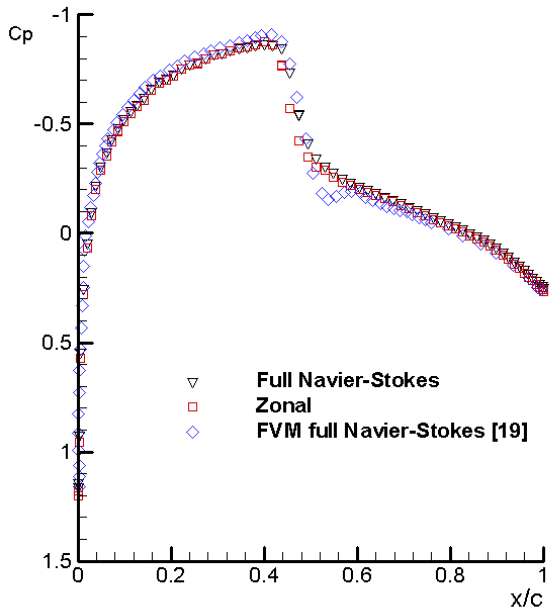

Fig. 4. Pressure coefficient over the NACA 0012 airfoil at $\alpha = 0^o$, $M_\infty = 0.8$ and Re=$9\text{x}10^6$.

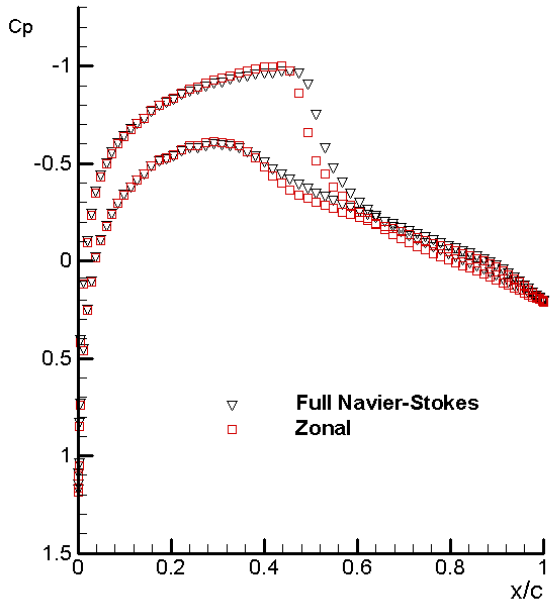

Fig. 5. Pressure coefficient over the NACA 0012 airfoil at $\alpha = 1.25^o$, $M_\infty = 0.8$ and Re=$9\text{x}10^6$.

Navier-Stokes result as shown in figure 4. These results are also in a fairly good agreement with the full Navier-Stokes result on a 320x64 grid obtained by a finite volume method [19]. The same conclusion can be drawn from the numerical results shown in figure 5 for the case of 1.25° angle of attack, M_∞=0.80 and Re=9x10^6. While the difference near the shock wave between the present full Navier-Stokes and the finite volume results may mainly be attributed to the grid resolution and different turbulence models, the difference between the present full Navier-Stokes and zonal results may be due to the accuracy of the potential approximation near the shock wave.

Calculations were also performed for a compressible flow around the RAE 2822 airfoil. The results for 2.92° angle of attack, $M_\infty = 0.725$ and Re=6.5x10^6 corresponding to the Case 6 of reference [20], are presented in figure 6. A grid of 217x65 is employed for the

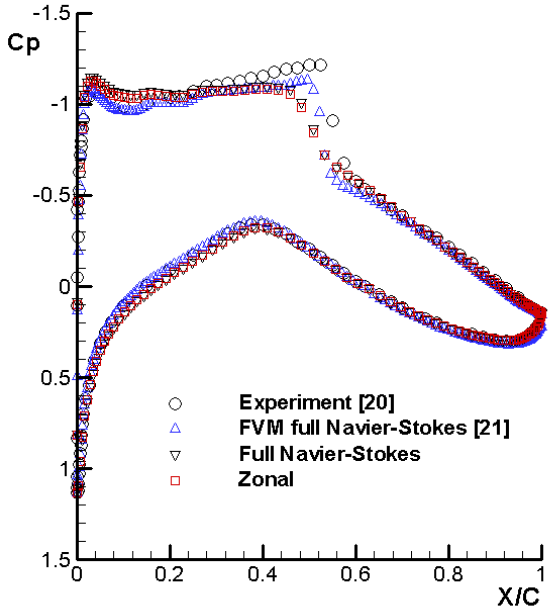

Fig. 6. Pressure coefficient over the RAE 2822 airfoil at $\alpha = 2.92^\circ$, $M_\infty = 0.725$ and Re=6.5x10^6.

present full Navier-Stokes and zonal solutions. For the zonal result, the 217x41 grid near the airfoil and its wake is chosen as the viscous zone and the 217x20 grid outside as the potential zone. The first grid point off the wall is at a distance of about 1x10^{-5} chords. Again the full Navier-Stokes and zonal solutions are in excellent agreement for the considered viscous flow. The grid resolution, different turbulence models, and different numerical methods may all contribute to discrepancy between the finite volume result [21] (using a grid of 369x65) and the current result.

It is concluded from the above discussion that the overall agreement between the full Navier-Stokes and zonal method is very good. However, significant computational time is saved by using the zonal method for the present two dimensional compressible and incompressible high Reynolds number turbulent flows. The author also believes that the interfaces could be placed closer to the airfoil surface and its wake. This will be investigated further.

5 Conclusions

A zonal finite element method has been developed in the present paper to simulate two-dimensional compressible and incompressible high Reynolds number external flows.

Numerical results presented for the two-dimensional turbulent flows around the NACA 0012 and RAE 2822 airfoils show that the coupling between the outer potential flow solution and inner viscous flow solution is successful, which is justified by the physical flow natures of the problems.

A streamline upwind Petrov-Galerkin finite element method is shown, in the present paper, to be equivalent to a Galerkin method applied to a modified transport equation.

Further investigation into the effects of the grid resolution and interface locations is needed before applying the approach to practical three-dimensional steady and unsteady aerodynamic problems.

References

[1] Metha, U. and Lomax, H. Reynolds-averaged Navier-Stokes computations of transonic flows. The state of the art. *Proceedings of Symposium on Transonic*

Perspective, ed. Nixon, D., Progress in Astronautics, Vol. 81, 1982.

[2] McCroskey, W. Unsteady airfoils. *Annual Review of Fluid Mech.*, Vol. 14, 1982.

[3] Le Balleur, J.C., Peyret, T., and Viviand, H. Numerical studies in high Reynolds number aerodynamics. *Computers and Fluids*, Vol. 8, No. 1, 1980.

[4] Le Balleur J.C. Numerical viscous-inviscid interaction in steady and unsteady flows. *Proceedings of the 2nd Symposium on Numerical and Physical Aspects of Aerodynamic Flows*, Long Beach, CA, 1983.

[5] Le Balleur, J.C. New possibilities of viscous-inviscid numerical techniques for solving viscous flow equations with massive separation. *Proceedings of the 4th Symposium on Numerical and Physical Aspects of Aerodynamic Flows*, Long Beach, CA, 1989.

[6] Le Balleur, J.C. and Girodroux-Lavigne, P. Calculation of fully three-dimensional separated flows with an unsteady viscous-inviscid interaction method. *Proceedings of the 5th Symposium on Numerical and Physical Aspects of Aerodynamic Flows*, Long Beach, CA, 1992.

[7] Sankar, L., Zibi-bailly, J., Le Balleur, J.C., Blaise, D., Rouzaud, O., and Rhee, M. A comparative study of three methodologies for modeling dynamic stall. *28th European Rotorcraft Forum*, Bristol, September 17-20, 2002.

[8] Brune, G.W., Rubbert, P.E., and Forester, C.K. The analysis of flow fields with separation by numerical matching. *AGARD-CP-168*, 1975.

[9] Cambier, L., Ghazzi, W., Veuillot, J.P., and Viviand, H. A multi-domain approach for the computation of viscous transonic flows by unsteady type methods. *Computational Methods in Viscous Flows*, ed. Habashi, W.G., Recent Advances in Numerical Methods in Fluids, Vol. 3, 1984.

[10] Su, J. Calculation of compressible and incompressible viscous flows by a viscous inviscid splitting finite element method. *ICAS 2002 Congress*, September 8-13, Toronto, Canada.

[11] Elkadri, N.E., Soulaimani, A., and Deschenes, C. A finite element formulation of compressible flows using various sets of independent variables. *Computer Methods in Applied Mechanics and Engineering*, Vol. 181, 2000.

[12] Soulaimani, A., Saad, Y., and Rebaine, A. An edge based stabilized finite element method for solving compressible flows: formulation and parallel implementation. *Computer Methods in Applied Mechanics and Engineering*, Vol. 190, 2001.

[13] Baruzzi, G.S., Habashi, W.G., Guevremont, J.G., and Hafez, M.M. A second order finite element method for the solution of the transonic Euler and Navier-Stokes equations. *International Journal for Numerical Methods in Fluids*, Vol. 20, 1995.

[14] Brooks, A.N. and Hughes, T.J.R. Streamline upwind/Petrov-Galerkin formulations for convection dominated flows with particular emphasis on the incompressible Navier-Stokes equations. *Computer Methods in Applied Mechanics and Engineering*, Vol. 32, pp 199-259, 1982.

[15] Spalart, P.R. and Allmaras, S.R. A one-equation turbulence model for aerodynamic flows. *AIAA-92-0439*, 1992

[16] Hafez, M., South, J., and Murman, E. Artificial compressibility methods for numerical solutions of transonic full potential equation. *AIAA Journal*, Vol. 17, pp 838-844, 1979.

[17] Nishida, B.A. Full simultaneous coupling of the full potential equation and the integral boundary layer equations in three dimensions. *Ph.D. Dissertation*, Massachusetts Institute of Technology, 1996.

[18] Abbott, I.H. and von Doenhoff, A.E. *Theory of Wing Sections*. Dover Publications, Inc., New York, 1959.

[19] Martinelli, L. Calculations of viscous flows with a multi-grid method. *Ph.D. Dissertation*, Princeton University, 1987.

[20] Cook, P.H., McDonald, M.A., and Firmin, M.C.P. Aerofoil RAE 2822 – pressure distributions, and boundary layer and wake measurements. *AGARD-AR-138*, 1979.

[21] Slater, J.W. NPARC alliance validation archive – RAE 2822 transonic airfoil. *NPARC Alliance CFD Verification and Validation Website*, 2002.